INTERNATIONAL JOURNAL OF HYDROGEN ENERGY 33 (2008) 1142–1152

Available at www.sciencedirect.com

ScienceDirect

journal homepage: www.elsevier.com/locate/ijhydene

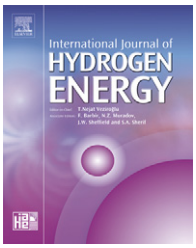

Review

Numerical modeling for preliminary design of the hydrogen production electrolyzer in the Westinghouse hybrid cycle

F. Jomard[a,*], *J.P. Feraud*[a], *J.P. Caire*[b]

[a]*Commissariat à l'Énergie Atomique/Valrhô, DTEC/SGCS/LGCI, BP 17 171, 30 207 Bagnols sur Cèze, France*
[b]*LEPMI, ENSEEG, 1130 Rue de la Piscine, 38 402 Saint Martin d'Hères, France*

ARTICLE INFO

Article history:
Received 15 November 2006
Received in revised form
18 October 2007
Accepted 18 December 2007
Available online 11 February 2008

Keywords:
Hydrogen
Hybrid cycle
Modelizing
Filter press
Electrolyzer
Nuclear
Generation IV
Overpotential
Flux-Expert

ABSTRACT

The Westinghouse sulfur process decomposes water into hydrogen and oxygen in several steps. This process requires a high-temperature thermal source, which could ideally be a fourth-generation nuclear reactor for recycling compounds. The process consists of producing hydrogen in a specific electrolyzer where protons are reduced at the cathode while an oxidation reaction, in which sulfur dioxide forms sulfuric acid, takes place in the anode compartment. This type of reaction enables mass hydrogen production at a very low cell voltage because the thermodynamic oxidation potential of SO_2/H_2SO_4 is 0.17 V, compared with 1.23 V for the common electrolysis of water by H_2O/O_2 oxidation. This article describes the electrical/thermal coupling of an individual filter press electrolysis cell for the preliminary design of a future test pilot. Solving coupled equations describing heat transfer and electrokinetics in the presence of forced convective flow of a two-phase electrolyte allows charge and heat transfer to be predicted for different configurations.

Contents

1. Introduction 1143
2. Hydrogen production 1143
3. The Westinghouse process 1144
   3.1. Westinghouse process flow sheet and operating procedure 1144
   3.2. The Westinghouse process electrolyzer 1145
   3.3. Selected electrolyzer geometry 1146
4. Numerical modeling of the electrolysis cell 1146
   4.1. Advantages of models developed with Flux *Expert*® 1146

*Corresponding author.
E-mail address: florentjfr@yahoo.fr (F. Jomard).
0360-3199/$ - see front matter © 2007 International Association for Hydrogen Energy. Published by Elsevier Ltd. All rights reserved.
doi:10.1016/j.ijhydene.2007.12.052

4.2. Physical models . . . 1147
4.2.1. Electrokinetic model. . . . 1147
4.2.2. Thermal model. . . . 1147
4.3. 2D electrolyzer meshing. . . . 1147
4.4. Main hypotheses of model. . . . 1147
4.5. Effect of hydrogen generated at the cathode and modeling . . . 1148
5. Numerical solution . . . 1149
5.1. Input data. . . . 1149
5.1.1. Modeling the secondary current distribution . . . 1149
5.1.2. Thermal modeling with forced convection . . . 1149
5.2. Modeling results. . . . 1149
6. Conclusions. . . . 1151
References . . . 1152

1. Introduction

Large-scale hydrogen production as a substitute for oil was widely investigated following the first two oil crises of the 1970s and 1980s [1–3]. This work came to an abrupt halt in the mid-1980s after a sharp drop in oil prices. The volume of hydrogen production remained sufficient to meet supply requirements, mainly for chemistry (ammonia synthesis, 60% of consumption) and petrochemistry (20% of consumption) [4].

The tensions currently being encountered on the energy market and global warming due to the release of carbon dioxide have led to renewed interest in dihydrogen as fuel given its high energy value and absence of pollution. The two fundamental difficulties that limit its use are its production cost and storage feasibility.

Concerning production costs, dihydrogen synthesis processes investigated in the 1970s are now being reexamined in the light of the Generation IV International Forum (GIF), chartered in July 2001 to lead the collaborative efforts of the world's leading nuclear technology nations to develop next-generation nuclear energy systems to meet the world's future energy needs.

Ten countries are working together to lay the groundwork for the fourth-generation nuclear reactor. Nuclear power plant technology has evolved in three distinct design generations: (I) prototypes, (II) currently operating plants, and (III) advanced reactors. The next generation of nuclear energy systems, generation IV, must be licensed, built, and operated in a manner that will provide a competitively priced supply of energy. They must consider optimum use of natural resources, while addressing nuclear safety, waste and proliferation resistance, and public perception concerns in the countries where those systems are deployed. In this framework, the new reactor technology should also open the way to very high operating temperatures (1000–1100 K) at which thermochemical hydrogen production becomes possible. This option has spurred renewed interest in synthesis cycles such as the Bunsen cycle [5] or the Westinghouse process hybrid cycle [1] coupling thermochemical and electrochemical systems. Compared with classical water electrolysis, these processes are considerably more complex to develop but should significantly diminish the energy necessary for large-scale hydrogen production by modifying the thermodynamic balance of the process. Together with nuclear energy, other high-temperature sources like solar energy are also promoted in a European framework, HYTHEC. This program, involving a restricted number of partners (six, in five countries), provides preliminary technical and economic assessments of an interesting route for future H_2 production, via promising CO_2 free thermochemical cycles: mainly the sulfur–iodine cycle and the Westinghouse sulfur cycle as an alternative "hybrid" solution [6].

The high temperatures could also be used in high-temperature electrolysis, also called steam electrolysis. This process is more efficient economically than traditional room-temperature electrolysis of water because some of the energy is supplied as heat, which is cheaper than electricity, and because the electrolysis reaction is more efficient at higher temperatures [7].

2. Hydrogen production

Although hydrogen is not directly available in nature, it can be produced using three major energy sources: fossil fuels, nuclear power, and renewable energy sources. To be economically and ecologically viable, however, hydrogen production must meet three criteria:

- *Competitiveness*: The production cost must not be too high: for example assuming the gasoline and hydrogen consumptions of vehicles were roughly equivalent, hydrogen energy would be competitive at $1.50/Gallon [8].
- *Optimum energy efficiency*: Hydrogen production must not entail excessive energy costs.
- *Environmental considerations*: The fabrication process must be relatively nonpolluting, particularly with regard to greenhouse gas emissions.

Several mass production methods are currently operational, but none of them to date completely fulfills all three criteria. About 95% of hydrogen is produced today from fossil fuels by catalytic reforming (a chemical reaction in which hydrocarbon molecules are broken down endothermically to release hydrogen). Among these processes, steam reforming of natural gas is a typical example of a mass production process that releases large quantities of carbon dioxide into the atmosphere and thus fails to meet current environmental criteria.

Nomenclature

Symbols

A	electrolyte free flow area, m^2
C_P	heat capacity at constant pressure, $J\,kg^{-1}\,K^{-1}$
F	Faraday's constant $= 96\,500\,C\,mol^{-1}$
h_t	heat transfer coefficient, $W\,m^{-2}\,K^{-1}$
I	electric current, A
JNF	current density normal to the boundary, $A\,m^{-2}$
j_0	exchange current density at equilibrium, $A\,m^{-2}$
j	local current density, $A\,m^{-2}$
k	thermal conductivity, $W\,m^{-1}\,K^{-1}$
M	atomic mass of $H_2 = 0.002\,kg\,mol^{-1}$
m_V	gaseous H_2 density $= 0.08988\,kg\,m^{-3}$
$\vec{n}$	normal vector
n	number of electrons
P	wetted perimeter, m
q	heat source density, $W\,m^{-3}$
q	electric power, W
Q_l	liquid flow rate, $L\,h^{-1}$
Q_g	gas flow rate, $NL\,h^{-1}$
r	electrical resistance, Ω
R	ideal gas constant $= 8.314\,J\,mol^{-1}\,K^{-1}$
Re	Reynolds number
S	stoichiometric coefficient
T	temperature, K
T_{amb}	ambient temperature, K
V_0	standard electrical potential, V
V	electrical potential, V

Greek symbols

α	symmetry factor
ε_g	gas volume fraction
ρ	density $kg\,m^{-3}$
σ	electrical conductivity, $S\,m^{-1}$
σ_{int}	equivalent electrical conductivity, $S\,m^{-1}$
μ	dynamic viscosity, $kg\,s^{-1}\,m^{-1}$
$\vec{v}$	velocity vector, $m\,s^{-1}$
v	velocity, $m\,s^{-1}$
η	overvoltage, V
η_c	cinematic viscosity, $m^2\,s^{-1}$
$\vec{\nabla}$	gradient

Over the longer term, the most ecological hydrogen production technology would be water electrolysis by electricity which does not come from a fossil fuel power plant. Technically, the process is fully mature and is already used in industrial applications (e.g. transports or portable devices) that do not require high production, as this synthesis method is costly given its high electrical consumption.

Since the founding of the GIF, the scientific community has examined several solutions for combining nuclear technology with large-scale hydrogen production; nuclear energy can be employed for hydrogen production according to three different approaches [9]:

- the use of excess electricity from nuclear reactors for direct water electrolysis;
- the direct use of heat from high-temperature nuclear reactors for thermochemical processes such as the iodine–sulfur cycle or steam methane reforming and the Ca–Br–Fe cycle [10];
- the combined use of high-temperature heat and electricity, as in the Westinghouse or Deacon hybrid processes [11].

3. The Westinghouse process

In 1967, Juda and Moulton [1] demonstrated the advantages of using sulfur dioxide in solution to diminish the activation overpotential during water electrolysis. The "Westinghouse process" was patented by Brecher in 1975 [12].

3.1. *Westinghouse process flow sheet and operating procedure*

The Westinghouse process is based on a hybrid sulfur redox cycle involving an electrochemical reaction to produce hydrogen and a thermochemical stage to produce oxygen. The complete cycle shown in Fig. 1 comprises an electrolyzer stage and three blocks corresponding to conventional chemical processes. The overall cycle yields 1 mol of hydrogen and half a mole of oxygen by decomposing 1 mol of water.

Oxygen is produced by high-temperature thermal cracking of sulfuric acid (step ① in Fig. 1):

$$H_2SO_4 \rightarrow H_2O + SO_2 + \tfrac{1}{2}O_2. \quad (1)$$

Sulfuric acid dissociates to form oxygen and sulfur dioxide at about 1000 K, a temperature fully compatible with some fourth-generation reactors.

After oxygen is recovered in the evaporator ②, the process continues in the electrolyzer ③ by an electrochemical reaction between sulfur dioxide and water to form hydrogen. The overall reaction is the following (2):

$$SO_2 + H_2O \leftrightarrow H_2SO_3 \quad \text{then } SO_2 + 2H_2O \rightarrow H_2 + H_2SO_4. \quad (2)$$

The voltage balance in an electrolyzer between the anode and cathode is expressed thus

$$V = V_0 + \eta_a + |\eta_c| + rI \quad (3)$$

and the electric power consumption P can be obtained as follows:

$$P = VI. \quad (4)$$

Eq. (3) does not integrate the concentration overpotentials which are negligible in the presence of forced convection in a plate electrolyzer. The electric power P, i.e. the energy demand and the process cost, depends on all the terms of Eq. (3). In this equation, the standard potential V_0 can be diminished by carefully choosing the electrochemical couple. The H_2SO_3/H_2SO_4 couple used in reaction (2) has a standard potential of only 0.17 V [13] compared with the standard potential of 1.23 V for water (H_2O/O_2); moreover in a standard water electrolysis cell the overall voltage can rise to 2.05 V for

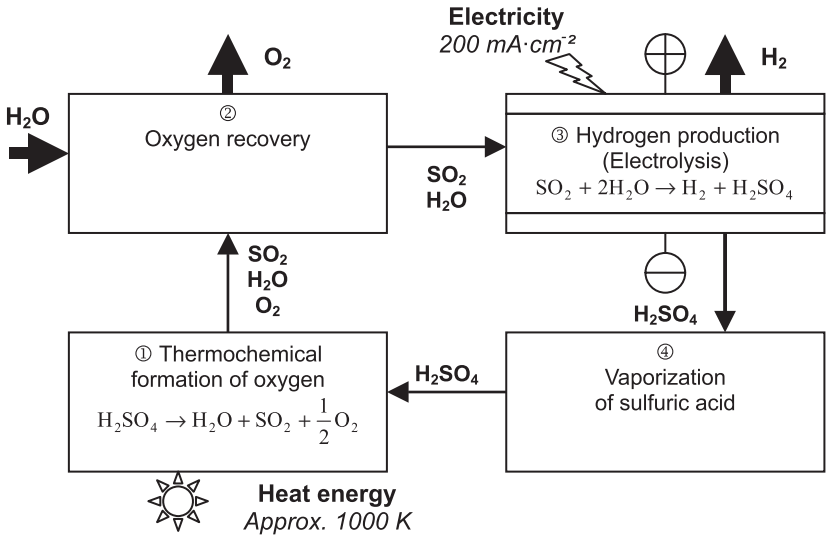

Fig. 1 – Simplified block diagram of the Westinghouse process.

a current density of 3 A [14]. Compared with water electrolysis, the electrochemical oxidation of SO_2 to H_2SO_4 thus divides by seven the electric power required in the anodic compartment. A similar reduction in electric power consumption can be expected for H_2 production by the Westinghouse sulfur cycle. The overpotential phenomenon [15] is an irreversible effect due to kinetic limitations appearing as a potential discontinuity at the electrode–electrolyte interface as seen in Fig. 5. The overpotential magnitude is related to the choice of electrolyte and electrode and to the current density (see Eq. (12)), so the energy losses related to overpotentials η_a and η_c can be reduced by suitably matching the electrode and electrolyte. Finally, the electric power consumption can also contribute to improving the ohmic losses inherent in the current flow. This can be obtained by modifying the electrolyzer geometry, the membrane properties (material, thickness, resistivity), the electrolyte, etc. In our case, the complexity of the thermal effects and couplings requires a good numerical model to optimize the electrolyzer reactor.

3.2. *The Westinghouse process electrolyzer*

The electrolyzer process is the heart of the Westinghouse sulfur cycle since it produces hydrogen by the cathodic reduction of sulfuric acid (5). A filter press electrolyzer design [15] (Fig. 2) was chosen as a good compromise in term of compactness and efficiency. The electron balance is achieved by the anodic oxidation of sulfur dioxide into sulfuric acid (6). The two half-cell reactions and the overall reaction are [16]:

$$\text{Cathode}: \quad 2H^+ + 2e^- \rightarrow H_2 \quad E_0 = 0.00\,\text{V}, \tag{5}$$

$$\text{Anode}: \quad SO_2 + 2H_2O \rightarrow 2H^+ + H_2SO_4 + 2e^- \quad E_0 = 0.17\,\text{V}, \tag{6}$$

$$\text{Total}: \quad SO_2 + 2H_2O \rightarrow H_2 + H_2SO_4. \tag{7}$$

The advantage of this process is that it requires much less electric power than direct water electrolysis (see Section 3.1),

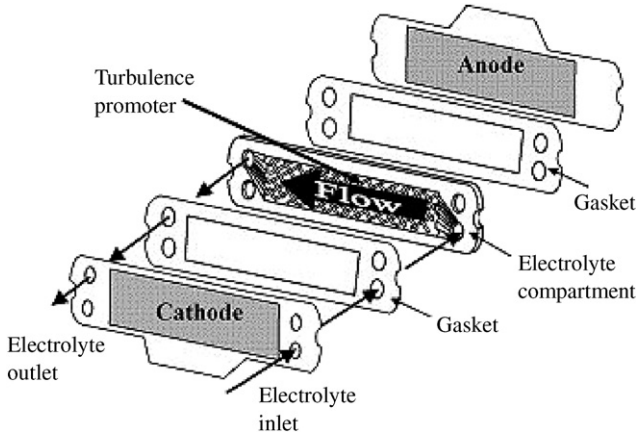

Fig. 2 – ICI FM01-LC electrolyzer.

although it is subject to technological constraints:

- *Side reactions*: Diffusion, then reduction of sulfur dioxide at the cathode [1,2]. This type of cathode reaction forms sulfide that poisons the cathode and diminishes the hydrogen formation. The solution for avoiding this problem is to use membranes to separate the anode from the cathode [14].
- *Anodic corrosion* [15]: The anode must be coated with gold or platinum-group metals.
- *Two-phase gas flow*: Managing the hydrogen gas release raises another technological difficulty. It is important to avoid any gas accumulation in the cathode compartment that would diminish the local current intensity and increase the pressure drop, and thus the energy consumption.

These technical considerations highlight the difficulty of designing a filter press electrolyzer such as the one presented in Fig. 2. Considering the cost and complexity of fabricating a pilot electrolyzer, numerical modeling proved to be a valuable tool for the preliminary design of a prototype unit.

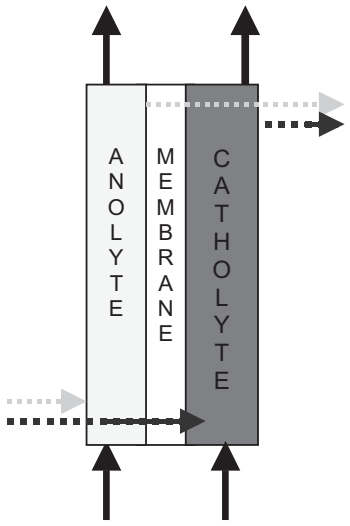

Fig. 3 – Model representation of a membrane-type filter press element.

The most suitable operating parameters for hydrogen production with a current density of about 2000 A m^{-2} were determined through a bibliographical survey: for a sulfur dioxide pressure of 1 bar (almost all the studies were carried out at this pressure) the sulfuric acid concentration should be about 50 wt% at temperatures between 25 and 90 °C [17,18].

3.3. *Selected electrolyzer geometry*

The selected prototype electrolyzer is a commercial FM01-LC filter press reactor manufactured by ICI Chemical & Polymers Company with an active surface area of 64 cm^2 [19,20].

A filter press electrolyzer is commonly arranged by stacking representative unit cells (Fig. 2) made up of a flat plate, the electrode, which is covered by two "inner" frames consisting of plastic nets which act as turbulence promoters. The fluid distributor is located upstream of the reaction zone in the "inner" frames. The "inner" frames are inserted into a polymeric "outer" frame. These representative unit cells have alternating anolyte and catholyte compartments, separated by membranes. An accurate description of the cell can be found elsewhere [21]. A conventional cell consists of two electrodes and two compartments separated by conductive membrane as shown in Fig. 3.

In this work an element of the actual cell is modeled by a system of two compartments separated by a membrane. To simplify the rate distribution modeling it is assumed that the electrolytes penetrate vertically, whereas in the actual filter press cell they should enter laterally, as shown by the grey arrows in Fig. 3.

4. Numerical modeling of the electrolysis cell

The purpose of this modeling study was to determine the optimum hydrogen production conditions versus the geometric parameters and operating conditions (flow rate, electric current, temperature, concentration, and pressure). Numerical modeling is a predictive approach that can also explain the phenomena observed. Once validated, the model limits the number of tests necessary to develop the process, with advantages in terms of cost, risk, and safety. Modeling saves time and money, and allows many different and sometimes complex configurations to be examined. Different operating configurations can thus be investigated with a relatively small number of tests through computer experiments [22] based on experimental design methodology [23] using a simple office computer.

The modeling results described here concern electrokinetic and heat transfer computations performed with the finite element code Flux Expert® [24].

4.1. *Advantages of models developed with Flux Expert®*

The overpotentials in the potential balance (3) correspond to a potential discontinuity at the electrode/electrolyte interface [15]. Modeling overpotentials raises a specific numerical problem that cannot be dealt with directly by a finite element code, which by definition assumes the continuity of the variable in this case the potential. In the case of the Westinghouse process, the cathodic and anodic overpotentials are small but must nevertheless be taken into account because their irreversible effects can impact the electrolyzer electrical consumption.

Few software tools are currently capable of modeling interface overpotentials, i.e. the electrical potential discontinuity between the electrolyte and the electrode interface. Flux Expert® can be used to compute both the primary and secondary electrical distribution, which assumes the overpotentials are taken into account [26] in the electrochemical cell. To solve this problem, the calculation code creates an interface of small but nonzero thickness (Fig. 4). The interface is considered as a transition zone of conductivity σ_{int} where electrokinetic equations are assumed applicable. This thickness, intended only to create the electrical potential jump, is taken into account through specific finite elements known as "interfacial elements", which are slipped between the electrolyte and the electrode but are not visible in the problem.

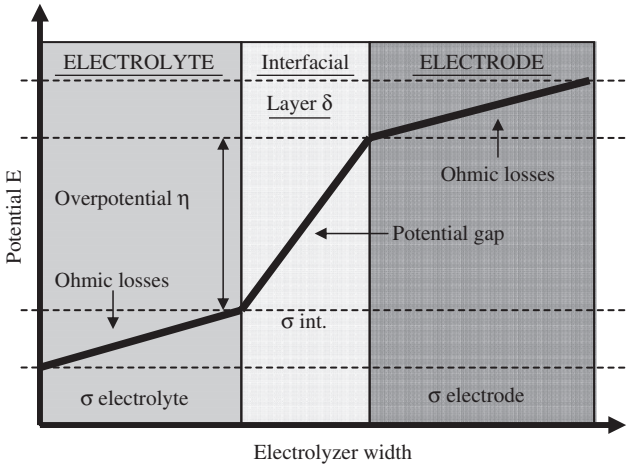

Fig. 4 – Overpotential model.

This method is described in the Flux Expert® documentation [24] and in the literature [25].

The purpose of this modeling study was to carry out the preliminary design for the prototype of an individual cell of the complete filter press electrolyzer.

4.2. *Physical models*

4.2.1. *Electrokinetic model*

The first equation to be solved corresponds to the Laplace equation (8), which is written as follows for any point in the electrical conductivity cell σ:

$$\vec{\nabla} \cdot (-\sigma \vec{\nabla} V) = 0. \tag{8}$$

The following types of limit conditions are possible at the cell boundaries:

$$\text{Presence of an insulator}: \quad -\sigma \vec{\nabla} V \cdot \vec{n} = 0, \tag{9}$$

$$\text{Current supply}: \quad -\sigma \vec{\nabla} V \cdot \vec{n} = \text{JNF}, \tag{10}$$

$$\text{Controlled potential}: \quad V = \text{constant}, \tag{11}$$

where $\vec{n}$ is the vector normal to the boundary $\partial\Omega$.

Solving Eq. (8) with conditions (9), (10), (11) yields a "primary" potential distribution. Assuming there are no interface overpotentials, the potential function is continuous at every point in the electrolyzer and the local current density $\vec{j}$ is calculated simply by applying Ohm's law:

$$\vec{j} = -\sigma \vec{\nabla} \cdot V \tag{12}$$

To obtain the secondary distribution from the primary distribution, allowance is necessary for the overpotential $\eta(\|\vec{j}\|)$ at the electrode/electrolyte interface, which depends on the local current density j according to the nonlinear Butler–Volmer law (13):

$$j = j_0(e^{\alpha n F \eta / RT} - e^{-(1-\alpha) n F \eta / RT}). \tag{13}$$

This nonlinear law reflects an irreversible phenomenon related to the presence of electrochemical reactions resulting in the potential jump as shown in Fig. 5. Allowance must be made for this interface discontinuity to properly compute the cell operating voltage that in turn determines the cell power consumption.

The overpotential law is defined in Flux Expert as a specific Fortran operator using a linear or logarithmic approximation of the Butler–Volmer law according to Eqs. (14) or (15):

$$\eta = A + B \log |j|, \tag{14}$$

$$\eta = A + B|j|. \tag{15}$$

In Eqs. (12) or (13) the A and B coefficients of the Tafel law were obtained from the literature [26]. The values implemented in the code are $A = 0.43$, $B = 4.3 \times 10^{-6}$ for anodic overpotential and $A = 0.0735$ and $B = -0.0394$ for cathodic overpotential.

4.2.2. *Thermal model*

The second step is to solve the thermal model. Heat transfer is described by the following equation valid throughout the cell Ω:

$$\rho C_P \frac{\partial T}{\partial t} + \rho C_P \vec{v} \cdot \vec{\nabla} T + \vec{\nabla} \cdot (-k \vec{\nabla} T) = q. \tag{16}$$

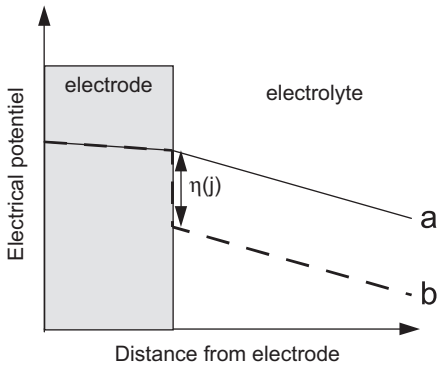

Fig. 5 – Primary (a) and secondary (b) potential distributions.

The thermal/electrokinetic coupling is implicit in Eq. (16) where the heat source term q is due to Joule effect losses evolving in each conductive zone in the cell:

$$q = \frac{\|J\|^2}{\sigma}. \tag{17}$$

Taking the overpotentials into account, the relation can be generalized to the whole cell as follows [27]:

$$q = (V - V_0)I + \eta_a I + \eta_c |I + rI^2, \tag{18}$$

where r is the global resistance and I the total current of the cell. Evaluating the terms of Eqs. (16)–(18) showed that all of them must be taken into account.

For an industrial cell the possible limit conditions at the boundary $\partial\Omega$ may be of the following types: Von Neumann (19), Dirichlet (20), or Fourier (21):

$$-k \frac{\partial T}{\partial \vec{n}} = 0, \tag{19}$$

$$T = \text{constant}, \tag{20}$$

$$-k \cdot \frac{\partial T}{\partial \vec{n}} = h_t(T - T_a). \tag{21}$$

4.3. *2D electrolyzer meshing*

The filter press reactor was modeled using the 2D refined grid in Fig. 7. The meshing was made of structured quadrangular elements which match particularly well the rectangular geometry. The grid used here contained 4000 nodes and was sufficiently accurate to minimize discretization errors.

4.4. *Main hypotheses of model*

The principal hypotheses adopted for these computations are the following:

- Electrolyzer dimensions $0.06 \times 0.0131 \times 0.16$ m ($e \times l \times h$).
- Modeling was performed in two dimensions along the length (l) and height (h). This hypothesis is justified by the geometry of the filter press: considering Fig. 1, it appears that the electrolyte flow is vertical although the electric current is horizontal; the side effects are negligible.

- The study was carried out under steady-state conditions.
- The physical properties (ρ, σ, k, C_P) of all the electrolyzer components are temperature-independent. Since the gas does not conduct electricity, the shielding effect of bubbles was taken into account via the Bruggeman equation (22) [28]. In contrast, the thermal conductivity of hydrogen ($0.172\,W\,m^{-1}\,K^{-1}$) is close to the electrolyte conductivity ($0.6\,W\,m^{-1}\,K^{-1}$), so the bubbles do not significantly modify the thermal conduction when the gas fraction and the temperature rise are limited. In this model the electrical conductivity coefficient depends locally on the gas fraction, but not the thermal coefficient k.
- The electrolytes are considered as a single-phase sulfuric acid solution. Nevertheless, the presence of many small-diameter (about 100 μm) hydrogen bubbles results in a shadow effect in the cathode compartment that diminishes the electrical conductivity. The local conductivity of the bath must therefore be recomputed according to the quantity of gas released while maintaining the characteristics of a single-phase fluid. The hypotheses concerning the presence of hydrogen are described in Section 4.5.
- All the outer walls of the electrolyzer are thermally insulated.
- Two fluids with different sulfuric acid concentrations pass through the vertical countercurrent electrolyzer at a constant rate. By limiting the problem to two dimensions, this flow is equivalent to planar flow.
- The Flux Expert® input data are representative of the operating conditions frequently described in the literature [11,12], i.e. a fluid inlet temperature of 323 K, a pressure of 1 bar, and sulfuric acid mass concentrations of 30% in the catholyte and 50% in the anolyte. A $2000\,A\,m^{-2}$ current density is fixed at the anode whereas a 0 V potential is imposed at the cathode.

4.5. *Effect of hydrogen generated at the cathode and modeling*

The catholyte conductivity is calculated by the Bruggeman equation (22) which depends on the gas volume fraction ε_g and the conductivity of the inlet electrolyte σ_0:

$$\sigma(h) = \sigma_0(1 - \varepsilon_g(h))^{3/2}. \quad (22)$$

The gas volume fraction depends on the hydrogen production (23), which in turn depends on the height of the electrolyzer (24):

$$\varepsilon_g(h) = \frac{Q_g(h)}{Q_g(h) + Q_l}, \quad (23)$$

where

$$Q_g(h) = \frac{S\,M\,1000\,3600\,e}{n\,F\,m_V} \int_0^h j(x)\,dx. \quad (24)$$

The hypotheses are that the gas generated at the cathode at level h is uniformly distributed within the cathode compartment at level h and that the current density is constant along the cathode, which is the case only if the gas volume fraction is everywhere less than about 10%. These hypotheses were verified from the results after computations.

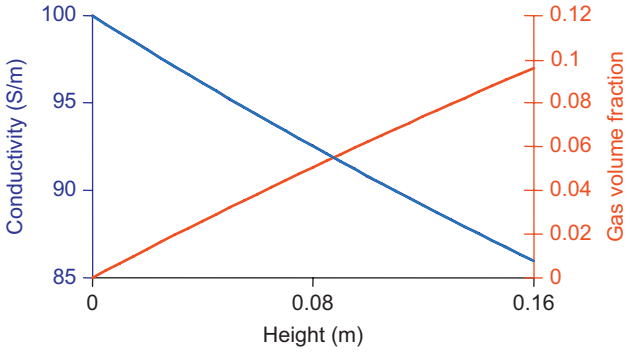

Fig. 6 – Gas volume fraction $\varepsilon_g(h)$ and electrical conductivity $\sigma(h)$ variations versus height on FM01-LC electrolyzer, where $j = 2000\,A\,m^{-2}$ and $Q_l = 50\,L\,h^{-1}$.

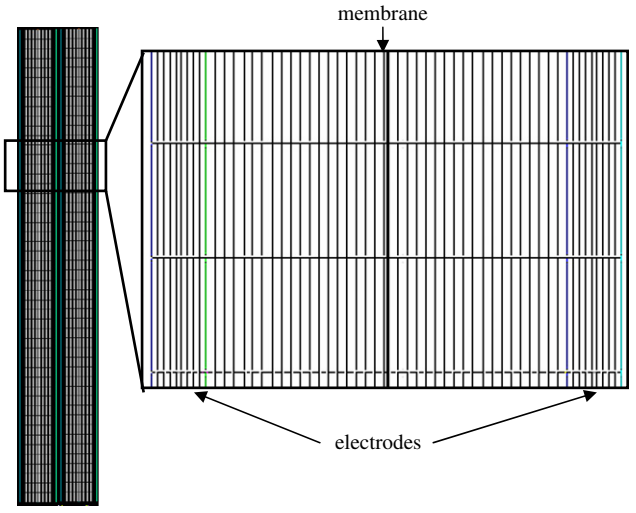

Fig. 7 – Electrolyzer grid meshing.

In the modeling study, the electrical conductivity σ_0 of the catholyte is $100\,S\,m^{-1}$. The conductivity and gas volume fraction in the catholyte are plotted versus the height in Fig. 6, showing that the gas volume fraction remains low (reaching only 9.5% at the top of the electrolyzer and validating the preceding hypothesis. As the gas volume fraction is low, the electrical conductivity variation range in the catholyte is also low, peaking at $100\,S\,m^{-1}$ at the bottom and $86\,S\,m^{-1}$ at the top.

In the cathode compartment, the fluid is accelerated by hydrogen bubbles released from the electrode. Under steady-state conditions the electrolyte flow rate is constant throughout the compartment, but the two-phase fluid velocity increases with h:

$$v(h) = \frac{v_{l,0}}{(1 - \varepsilon_g(h))}. \quad (25)$$

The flow behavior must be assessed by calculating the Reynolds number with the following expression:

$$Re = \frac{vD}{\eta_C} = \frac{\rho v D}{\mu}. \quad (26)$$

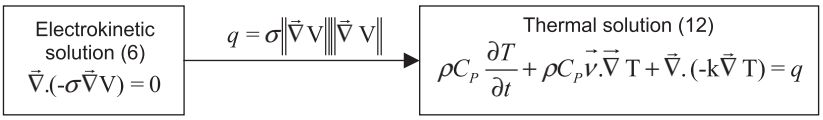

Fig. 8 – Coupling principle.

For a noncircular section the equivalent diameter D is given by

$$D = 4 \times \frac{A}{P}. \quad (27)$$

For a 0.05 $m^3 h^{-1}$ electrolyte flow rate the Reynolds number ranged from 650 to 730 whereas the hydrogen volume fraction did not exceed 10%. Reynolds numbers below 2000 ensure that the flow was laminar throughout the cell. Indeed, fluid dynamics can be computed with the Flux Expert® finite element code only if the Reynolds number is not turbulent. Two-phase flow modeling under turbulent conditions requires a finite-volume code such as Fluent® or Fluidyn®.

5. Numerical solution

The solution was obtained in two steps. The first was to model the electrochemical phenomena. Electrokinetic losses by Joule effect q are heat sources for modeling thermal effects as shown in Fig. 8. The model performs partial coupling between the electrokinetics, heat transfer, and two-phase fluid mechanics through heat sources q and the two-phase fluid velocity $v(h)$ defined in Eq. (25). Partial coupling is justified insofar as the quantity of gas in the cathode compartment remains low.

5.1. *Input data*

5.1.1. *Modeling the secondary current distribution*

The Laplace equation (6) was solved on a cross section measuring 0.0131 × 0.16 m. The calculations were performed by applying limit conditions at the boundary on the right edge of the anode (8) and the left edge of the cathode. The secondary current distribution is characterized by potential discontinuities at the electrolyte/electrode interfaces. The computational limit conditions are indicated in Fig. 9.

Based on the Faraday equation (18) and assuming 100% electrical efficiency, the global amount of hydrogen Q_g evolving at the cathode can be determined by

$$Q_g = \frac{S\,M\,1000 I\,3600}{n\,F\,m_V}. \quad (28)$$

In this equation for $S = 1$, $I = 12.88$ A, $n = 2e^-$ exchanged, the hydrogen production should be 5.34 NL h^{-1}, leading to a power consumption of 1.9 kWh Nm^{-3} per unit volume. This is much lower than the value of 4.25 kWh Nm^{-3} (34 kWh for 8 $Nm^3 h^{-1}$ of hydrogen) reported for the electrolyzer using alkaline electrolyte in the HARI project [29]. The Westinghouse process electrolyzer operating at 2000 A m^{-2} would thus gain a factor 2 with respect to conventional water electrolysis. Nevertheless, the total hybrid power must take thermochemical heating into account for recycling compounds, which is not detailed here.

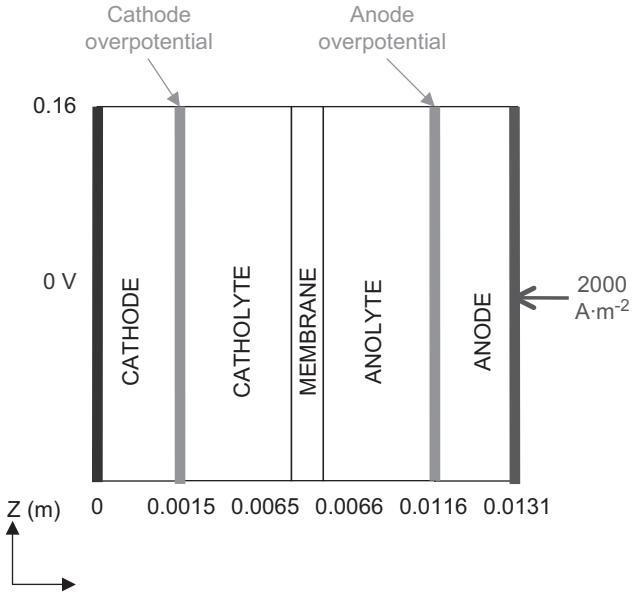

Fig. 9 – Electrokinetic model: dimensions (m) and limit conditions (not to scale).

5.1.2. *Thermal modeling with forced convection*

The electrolyzer was assumed to operate in countercurrent mode like a plate-type heat exchanger, ensuring satisfactory heat exchange transfers. The electrolyte inlet flow velocity was set at 0.069 m s^{-1} which corresponds, for the ICI FM01-LC cell, to a 0.05 $m^3 h^{-1}$ flow rate and provides a maximum hydrogen content of 10 vol% in the bulk electrolyte. Forced convection heat transfer must be taken into account in the model to properly simulate the thermal operation of the electrolyzer in the Westinghouse process. The electrokinetic/thermal coupling has to include the Joule effect losses computed from the electrokinetic model (18). The electrolyzer walls were assumed thermally insulated and Von Neumann (19) and Dirichlet (20) boundary conditions were used as shown in Fig. 10.

5.2. *Modeling results*

The secondary potential distribution (Fig. 11) was obtained using the nonlinear solver in Flux Expert® to take into account the nonlinear overpotentials. Fig. 11-clearly shows the potential jumps expected at the electrode/electrolyte interfaces. As the electrical potential is relatively constant along the height, only the central part of the electrolyzer is shown in the figure. Under these conditions the ohmic drop in

the individual electrolyzer cell was less than 0.3 V, and the anode overpotential appears as the main cause of the potential increase between the cathode and anode.

The value of the potential jump depends on the type of electrode, the electrolyte, and the physical properties (temperature, concentration, and pressure) of the electrolyte; in our case they represent 73% of the total cell voltage, making this the main parameter to be optimized to diminish the electric power necessary for hydrogen production. As the overpotentials depend directly on the current density, the value of 2000 A m^{-2} selected here thus appears to be a maximum rating.

To assess the effect of hydrogen bubbles, Fig. 12 compares the electrical potential lengthwise along the cathode compartment with and without allowance for the release of hydrogen bubbles. It reveals a very slight increase in the electrical potential in contact with gas, due to a drop in the electrical conductivity. Without gas, the catholyte conductivity is 100 S m^{-1}, but when gas is present this value drops to 93 S m^{-1} at a height of 0.08 m in the electrolyzer. As expected, Fig. 10 shows that the cell voltage is limited to a very low 0.80 V compared with other types of electrolysis [30]. Indeed Hamdani et al. [31] obtained a total cell voltage of 1.5 V for 2000 A m^{-2} current density using Li−Co_3O_4 electrocatalytic properties on the anodic reaction of alkaline water electrolysis. In our conditions, the electrolyzer required 50% less electric power. To prevent accelerated corrosion of the electrodes the temperature must be maintained as low as possible in the electrolyzer; for this purpose the heat dissipated by Joule effect and by electrode irreversibility must be estimated. Fig. 13 shows the dissipated power distribution in the electrolyzer compartments calculated from Eq. (17). Fig. 14 indicates a low temperature rise since the sum of the power dissipated in the electrolyzer is limited to 0.3 W. The two electrolytes account for more than 95% of the power total dissipated, and the heat dissipated in the membrane is very limited. This is an important consideration, as the membrane is already subject to mechanical stresses by fluid flow and could quickly be damaged in case of a large temperature rise. The anode compartment receives 10% more energy than the cathode compartment; this can be attributed to the difference in the acid concentrations in the two compartments.

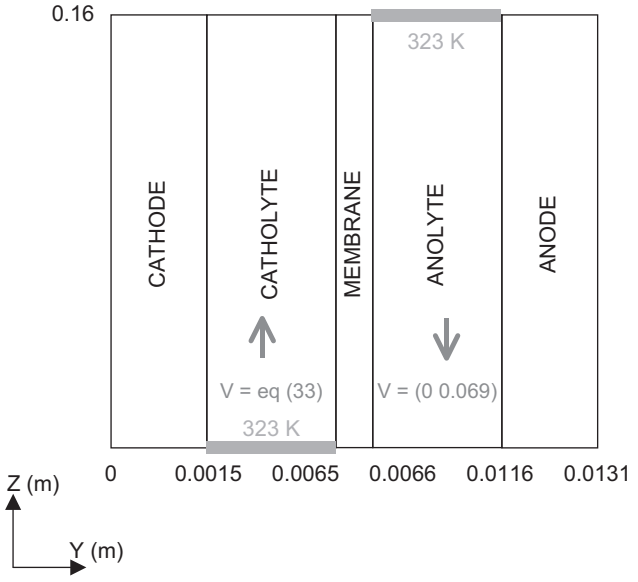

Fig. 10 – Thermal model: dimensions (m) and limit conditions (not to scale).

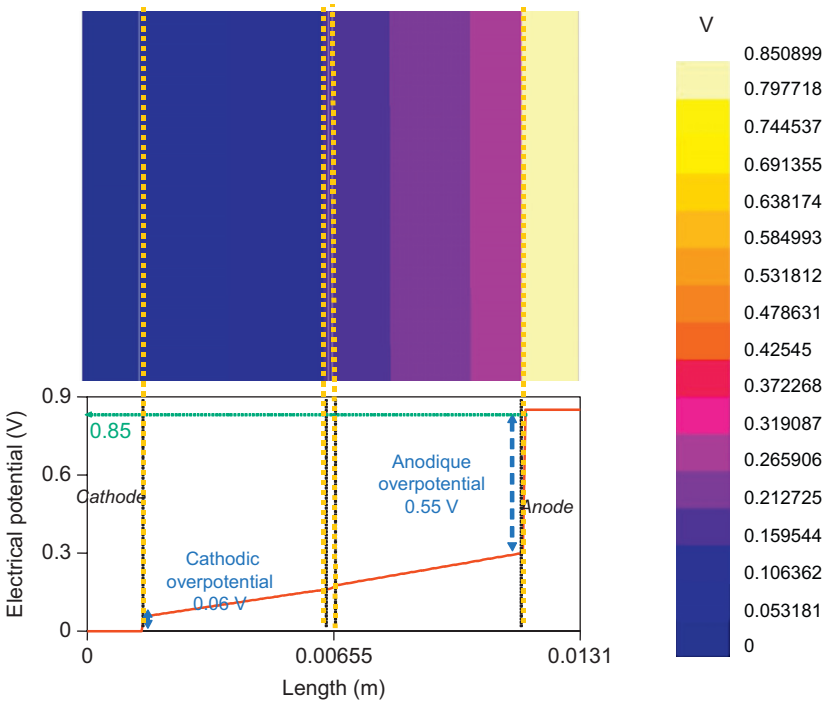

Fig. 11 – Electrical potential gradient (V) and horizontal cross section of electrical potential at height z = 0.08 m.

The thermal calculation in Fig. 14 indicates the temperature variation in both compartments and shows that bubbles have little effect on the temperature rise phenomena. The very slight temperature drop in the presence of gas was attributed to the higher velocity of the two-phase flow in the cathodic compartment calculated above (Eq. (25)).

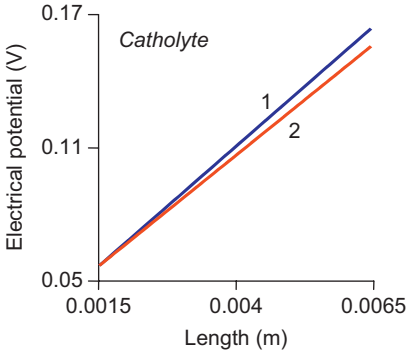

Fig. 12 – Electrical potential in cathode compartment height of 0.08 m: (1) in presence of gas (2) without gas.

The parabolic temperature curves reach a maximum at the center of the electrolyzer. This can be attributed to the counter-current fluid flow, coupled with a temperature rise in the media by Joule effect. The temperature rise between the hottest point and the fluid inlets is 6 K, as computed with Flux Expert® with no allowance for chemical reactions among the constituents. To determine the actual temperature difference between the coldest point (liquid inlet) and the hottest, allowance must be made both for heat sources generated by losses by Joule effect and for electrochemical reactions in the electrolytes.

6. Conclusions

Equations developed using the interface elements of Flux Expert® were used to solve coupled electrokinetic and heat transfer equations for a filter press reactor. The initial results showed that an elementary cell of a Westinghouse cycle electrolyzer could operate at a voltage lesser than 0.8 V for a current density of 2000 A m^{-2}, while maintaining a gas concentration of less than 10% and limiting the temperature

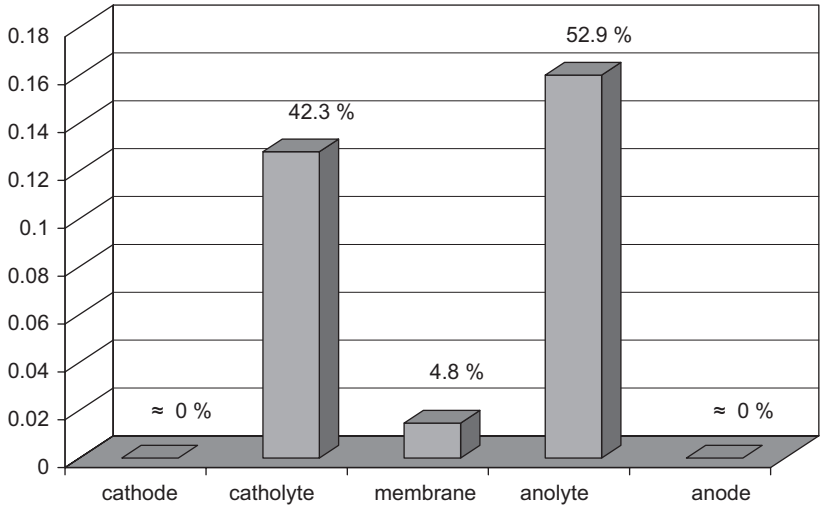

Fig. 13 – Power (W) dissipated by Joule effect.

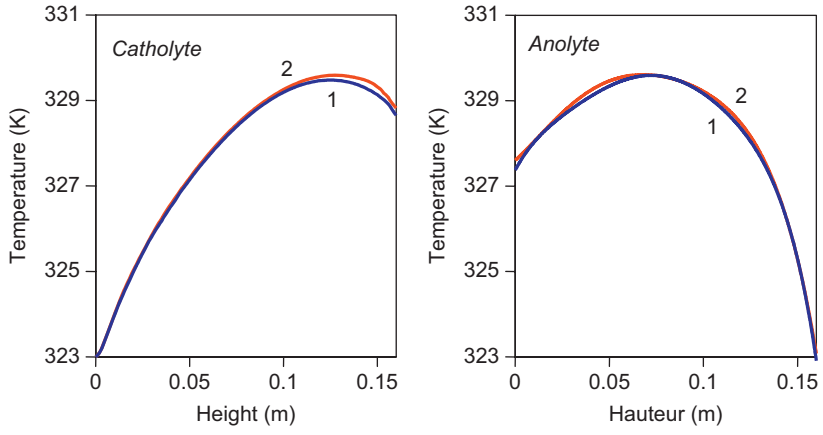

Fig. 14 – Temperature along the catholyte and anolyte: (1) in contact with gas (2) without gas.

rise to less than 6 K. Under these conditions, this initial modeling approach ensures that the process, though not yet optimized, is very efficient and appears competitive with other candidate processes for mass hydrogen production. In this preliminary design, the heat dissipated in the membrane remains very limited and should ensure a satisfactory operating life.

This preliminary study provides the first indications of an approach for optimizing the elementary cell. The next step will take into account more precise measurements of the overpotentials and the influence of the temperature and concentration on the physical parameters of the electrolytes [32]. These measurements can be included in the optimization of an elementary cell by Response Surface Methodology based on designs of computer experiments [33].

To go beyond the simplified hypotheses postulated in this study, work is now in progress to couple the Flux Expert® and Fluent calculation codes to take into account electrokinetics, fluid mechanics, and thermal phenomena in two-phase media under turbulent conditions. It will be also interesting to take into account the new Tafel law obtained by the recent work of Sivasubramanian et al. [13].

REFERENCES

[1] Brecher LE, Spewock S, Warde CJ. The Westinghouse sulfur cycle for the thermochemical decomposition of water. Int J Hydrogen Energy 1977;2:7–15.

[2] Struck BD, Junginger R, Boltersdorf D, Gehrmann J. The anodic oxidation of sulfur dioxide in the sulfuric acid hybrid cycle. Int J Hydrogen Energy 1980;5:487–97.

[3] Takehara Z, Nogami M, Shimizu Y. New electrolytic process in hybrid sulphur cycle for hydrogen production from water. Int J Hydrogen Energy 1989;14(4):233–9.

[4] Maurice B. Cours de chimie minérale. Paris: Dunod; 1990.

[5] Nomura M, Fujiwara S, Ikenoya K, Kasahara S, Nakajima H, et al. Application of an electrochemical membrane reactor to the thermochemical water splitting IS process for hydrogen production. J Membrane Sci 2004;240:221–6.

[6] Le Duigou A, Borgard JM, Larousse B, Doizi D. HYTHEC: an EC funded search for a long term massive hydrogen production route using solar and nuclear technologies. Int J Hydrogen Energy 2007;32:1516–29.

[7] Martinez-Frias J, Pham A-Q, Aceves SM. A natural gas-assisted steam electrolyzer for high-efficiency production of hydrogen. Int J Hydrogen Energy 2003;28:483–90.

[8] Sampson J. Replacing gasoline; alternative fuel for light-duty vehicle. OTA-E 364, September 1990.

[9] Yildiz B, Kazimi MS. Efficiency of hydrogen production systems using alternative nuclear energy technologies. Int J Hydrogen Energy 2006;31:77–92.

[10] Nakayama T, Yoshioka H, Furutani H, Kameyama H, Yoshida K. A bench-scale plant for producing hydrogen by the UT-3 thermochemical decomposition cycle. Int J Hydrogen Energy 1984;9:187–90.

[11] Simpson M, Herrmann S, Boyle B. A hybrid thermochemical electrolytic process for hydrogen production based on the reverse Deacon reaction. Int J Hydrogen Energy 2006;31:1241–6.

[12] Brecher LE, Electrolytic decomposition of water. United States Patent, 3 888 750, 1975.

[13] Sivasubramanian P, Ramasamy RP, Freire FJ, Holland CE, Weidner JW. Electrochemical hydrogen production from thermochemical cycles using a proton exchange membrane electrolyzer. Int J Hydrogen Energy 2007;32:463–8.

[14] Yurum Y. Hydrogen energy system: production and utilization of hydrogen and future. Berlin: Springer; July 1995 ISBN-10: 07 92 336 011.

[15] Coeuret F, Storck A. Éléments de génie électrochimique, Technique & Documentation. Paris: Lavoisier; 1993.

[16] Struck BD, Junginger R, Neumeister H, Dujka B. A three-compartment electrolytic cell for anodic oxidation of sulfur dioxide and cathodic production of hydrogen. Int J Hydrogen Energy 1982;7:43–9.

[17] Appleby AJ, Pinchon B. Electrochemical aspects of the $H_2SO_4-SO_2$ thermoelectrochemical cycle for hydrogen production. Int J Hydrogen Energy 1980;5:253–67.

[18] Appleby AJ, Pichon B. The mechanism of the electrochemical oxidation of sulphur dioxide in sulphuric acid solutions. J Electrochem Soc 1979;95:59–71.

[19] Trinidad P, Walsh FC. Hydrodynamic behaviour of the FM01-LC reactor. Electrochim Acta 1996;4:493–502.

[20] Bengoa C, Montillet A, Legentilhomme P, Legrand J. Characterization and modeling of the hydrodynamic behaviour in the filter-press type FM01-LC electrochemical cell by direct flow visualization and residence time distribution. Ind Eng Chem Res 2000;39:2199–206.

[21] Montillet A, Comiti J, Legrand J. Application of metallic foams in electrochemical reactors of filter-press type part I: flow characterization. J Appl Electrochem 1993; 23:1045.

[22] Sacks J, Schiller SB, Welch WJ. Design for computer experiments. Technometrics 1989;31:41–7.

[23] Box GEP, Draper N. Empirical model-building and response surfaces. New York: Wiley; 1987.

[24] FLUX-EXPERT: manuel métier électrochimie. Release 3.0, SIMULOG, 2000.

[25] Caire JP, Roustan H, Nicolas F, Pham P. Modelling coupled transfers in an industrial fluorine electrolyzer. J Appl Electrochem 1998;28:237–43.

[26] Farbman GH. The Westinghouse sulfur cycle hydrogen production process: program status. In: Vezroglu TN, Seifritz W., editors. Hydrogen energy systems, vol. 51. Oxford; Cambridge: 1979.

[27] Rousar I, Micka K, Kimla A. Electrochem Eng vol. 1, 2. Amsterdam: Elsevier; 1986.

[28] Nishiki YI. Effect of gas evolution on current distribution and ohmic resistance in a vertical cell under forced convection conditions. J Appl Electrochem 1986;16:615–25.

[29] Little M, Thomson M, Infield D. Electrical integration of renewable energy into stand-alone power supplies, incorporating hydrogen storage. Int J Hydrogen Energy 2007;32:1582–8.

[30] Vetter K. Electrochemical kinetics. New York: Academic Press; 1967.

[31] Hamdani M, Pereira MIS, Douch J, Addi AA, Berghoute Y, Mendonca MH. Physicochemical and electrocatalytic properties of $Li-Co_3O_4$ anodes prepared by chemical spray pyrolysis for application in alkaline water electrolysis. Electrochim Acta 2004;49:1555–63.

[32] Bengoa C, Montillet A, Legentilhomme A, Legrand J. Flow visualization and modelling of a Filter-press type electrochemical reactor. J Appl Electrochem 1997;27: 1313–22.

[33] Box GEP, Hunter WG, Hunter JS. Statistics for experimenters. New York: Wiley; 1978.